This item is the archived peer-reviewed author-version of:

Water management in an alkaline fuel cell

Ivan Verhaert[a,b,c,*], Sebastian Verhelst[a], Griet Janssen[b], Grietus Mulder[c],
Michel De Paepe[a]

[a]Department of Flow, Heat and Combustion Mechanics, Ghent University - UGent,
Sint-Pietersnieuwstraat 41, 9000 Gent, Belgium
[b]KHKempen, University College, Kleinhoefstraat 4, 2440 Geel, Belgium
[c]VITO, Flemish Institute for Technological Research, Boeretang 200, 2400 Mol, Belgium

Abstract

Alkaline fuel cells are low temperature fuel cells for which stationary applications, like cogeneration in buildings, are a promising market. To guarantee a long life, water and thermal management has to be controlled in a careful way. To understand the water, alkali and thermal flows, a model for an alkaline fuel cell module is developed using a control volume approach. Special attention is given to the physical flow of hydrogen, water and air in the system and the diffusion laws are used to gain insight in the water management. The model is validated on the prediction of the electrical performance and thermal behaviour. The positive impact of temperature on fuel cell performance is shown. New in this model is the inclusion of the water management, for which an extra validation is performed. The model shows that a minimum temperature has to be reached to maintain the electrolyte concentration. Increasing temperature for better performance without reducing the electrolyte concentration is possible with humidified hot air.

Key words: Alkaline Fuel Cell, Model, Heat Management, Water Management, Cogeneration, Performance

*Corresponding Author:
Email addresses: `ivan.verhaert@khk.be` (Ivan Verhaert)

Nomenclature

(hA)	overall conductance (W/K)
A	effective area of the fuel cell (m^2)
D	Diffusion constant (m^2/s)
E_{Nernst}	thermodynamic potential (V)
F	molar flow rate (kmol/hr)
Far	constant of Faraday (C/mol)
G	Gibbs free energy (GJ/kmol)
h	total enthalpy (GJ/kmol)
I	load current (A)
N_i	molar flux $(mol/m^2 \cdot s)$
p_I	(partial) pressure of flow I(bar)
P	power (W)
Q	heat (W)
R	universal gas constant (J/mol.K)
T	temperature (°C)
U	voltage (V)
v	velocity (m/s)
y_i	molar fraction of species i(-)
z	1-dimensional coordinate of location in the diffusion layer (m)
Re	Reynolds number (-)
Nu	Nusselt number (-)
c_j	coefficient j for the electrochemical model (*)
α	transfers coefficient (-)
η	overvoltage (V)
Subscripts	
an	anode
cat	cathode
FCB	fuel cell body
e	electrical
el	electrolyte
surr	surroundings
w	water/water vapour
A,B,...	identification of flow

2

1. Introduction

In a changing climate of energy supply and demand, distributed generation will play a significant role in our energy market [1]. Despite efforts in improved insulation and air tightness, building heating is still responsible for a large part of energy use in the world. In this prospect micro combined heat and power (micro-CHP) systems for building applications are getting more attention [2, 3]. Compared to other technologies fuel cell based systems offer a high power to heat ratio even at small sizes, because they are modularly built. Therefore, fuel cell based micro-CHP have the potential to reduce gas emissions and primary energy use in residential dwellings or buildings with a relatively low heat demand [4, 5, 6]. Four prominent fuel cell technologies are suitable as micro-CHP for building applications: solid oxide fuel cells (SOFC), proton exchange membrane fuel cells (PEMFC), phosphoric acid fuel cells (PAFC) and alkaline fuel cells (AFC) [7]. This last one is often forgotten since the surge of interest in PEMFC and SOFC [8]. Despite a lower amount of research and development activities, the AFC shows some interesting prospects such as cheaper construction, as it can be produced by relatively standard materials and does not require precious metals [8, 9]. The perceived disadvantage of carbon dioxide intolerance was found to be a minor problem. Next to several cost-effective solutions for carbon dioxide removal [5], in recent publications also a carbon dioxide tolerance of the AFC was found [8, 10]. This led to renewed interest in AFC technology [5, 9]. Next to lifetime improvements and handling degradation, the biggest advancements and reduction in total environmental impact are to be expected in reducing catalyst loading and optimising the overall system [5]. To optimise the overall system of an AFC-based micro-CHP for buildings it is necessary to understand the complete thermodynamic behaviour of the fuel cell. In previous work a model of an alkaline fuel cell was built in Aspen Custom Modeller [11]. The model combined prediction of electrical performance and thermal behaviour, but had no interest in water management, since re-concentrating the electrolyte solution can be easily implemented into the AFC-system, compared to the complex water

3

management within PEMFC [10]. However, if a more compact system design is desired to reduce material cost, the electrolyte concentration needs to stay within limitations for a longer period of time, to allow implementation of a smaller buffer tank. For this an understanding of the water management is necessary.

The objective of this study is to build a model which provides insight in the water management of the fuel cell and to study new control strategies for an AFC system.

2. Model development

2.1. Review of previous models

#### 2.1.1. General operation of an alkaline fuel cell

An overview of the general operation of an AFC system is given in [12]. As shown in Figure 1 an AFC operates by introducing hydrogen at the anode and oxygen/air at the cathode.

- At the hydrogen inlet a gas mixture of water vapour and hydrogen enters the gas chamber of the fuel cell. The hydrogen diffuses out of the gas chamber into the working area of the anode.

- At the oxygen inlet CO_2-free air or pure oxygen arrives in the gas chamber. The oxygen diffuses into the working area of the cathode to take part in the reaction.

Both electrodes, anode and cathode, are separated by a circulating electrolyte, a 6M potassium hydroxide solution (Fig.1).

[Figure 1 about here.]

At the anode hydrogen reacts with hydroxyl ions into water and free electrons, Eq. (1):

$$H_2 + 2(OH)^- \longrightarrow 2H_2O + 2e^- \tag{1}$$

4
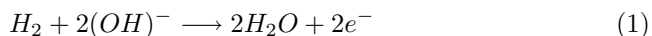
Within the electrolyte, the water is transported from the anode to the cathode. An external electric circuit leads the electrons to the cathode. At the cathode oxygen reacts with water and electrons into hydroxyl ions, Eq. (2):

$$H_2O + \frac{1}{2}O_2 + 2e^- \longrightarrow 2(OH)^-$$
(2)
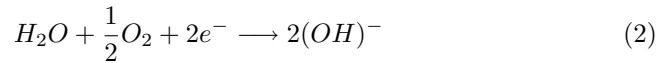
These ions flow from cathode to anode through the electrolyte, to sustain the total electrochemical reaction. Combining both reactions the overall reaction, Eq. (3), shows that the end product is water, which can be removed in one or both gas streams or in the electrolyte, depending on the fuel cell configuration.

$$H_2 + \frac{1}{2}O_2 + 2e^- \longrightarrow H_2O$$
(3)
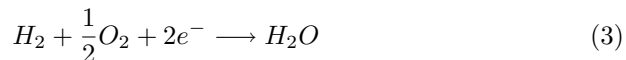
The overall reaction is exo-energetic. This energy has an electric part, which is transferred in the external electric circuit, and a thermal part, which results in a temperature rise inside the fuel cell. To maintain the overall fuel cell temperature, heat is removed by outlet mass flows or by losses to the environment.

2.1.2. Overview of AFC models

In order to improve fuel cell performance, mathematical models were developed which were able to predict electrical power. In the early nineties Kimble and White proposed a model for a complete fuel cell, where they take into account the polarization and physical phenomena going on in the solid, liquid and gaseous phase of both anode, separator and cathode regions, assuming a macro homogeneous, three-phase porous electrode structure [13]. The model divides the fuel cell in five layers, a gas diffusion layer and reaction layer for both anode and cathode and a separator, containing the electrolyte. In 1999 this model was the basis for the model of Jo and Yi, where they corrected some invalid correlations and parameters e.g. in the open-circuit potential and the liquid diffusion parameters [14]. Both Kimble and White and Jo and Yi used immobilized or re-circulating electrolyte and removed water in the gas streams. In 2006 Duerr et al. translated the model of Jo and Yi to a stack-model in a Matlab/Simulink environment and added dynamics to the electrical part of the

model [15]. Few details were given on the calculation method and the estimation method of some physical parameters. These models are all meant to predict the polarization curve or electric response of the fuel cell. In 1998 Rowshanzamir et al. studied the mass balance and water management in the AFC [16] by only applying mass balances and diffusion laws (Stefan-Maxwell) for the gas diffusion layer. However, their model does not provide any prediction on fuel cell performance. In earlier work a model was presented predicting both electrical performance and thermal behaviour [11]. This model will be used as a starting point to include the water management of the fuel cell.

In all the previous models the water was assumed to be disposed into the gas streams, either into one or into both. This assumption was the consequence of the used alkaline fuel cell type, with or without circulating electrolyte, the desired working point and/or the scope of the model. The fuel cell (system) in our research removes water by both exhaust gases and electrolyte flow. After the fuel cell, all these streams are collected in one reservoir, where eventually at nominal working point, the air flow is responsible for the disposal of water (vapour). Therefore in a first approach the water removal is modelled to happen in the gas streams [11].

In this work, the possibility of water disposal into the electrolyte, is included, in order to predict the water management within the stack allowing to generate intelligent control strategies in the future.

2.2. General equation and model assumptions

The model is divided into 5 areas, each with their own physical and thermodynamic behaviour. For each control volume the mass and energy balance are posed. Next to this, the following assumptions were made:

- Dynamic pressure losses within the fuel cell are neglected. In this way the total pressure can be assumed constant over the entire fuel cell. The same approach is used for a PEM fuel cell in [17], which is more critical than AFC to pressure drops, because it has no liquid electrolyte.

6

- The temperature is assumed to be uniform in each control volume and all output flows have this temperature, which is similar to the approach in [11, 17].

- The partial pressures within the gas chambers are the mean (partial) pressures of the input and output flow in the direction of the gas channels.

- The heat losses from the gas chambers to the environment are neglected, because the heat transfer surface is relatively small. All heat losses to the environment are therefore modelled as heat losses of the fuel cell body to the environment.

The five parts which are considered in the control volume model, are the anode and cathode gas chambers (AGC and CGC), the anode and cathode gas diffusion layers (AGDF and CGDF) and the fuel cell body (FCB), where the reaction takes place (See Fig.2). The model is modularly built. In this way a more detailed model can be obtained by serially connecting several individual models. Table 1 gives an overview of the molar and energy flows shown in figure 2. New elements in this model, compared to earlier work [11] are

- that the hydrogen and oxygen consumption and the water vapour removal of the fuel cell model is based upon diffusion laws. The diffusion is described by the Stefan-Maxwell equation, Eq.(4):

$$\frac{dy_i}{dz} = \frac{RT}{P} \cdot \sum_j \frac{y_i \cdot N_j - y_j \cdot N_i}{D_{ij}} \tag{4}$$

In this equation, the z-coordinate represents the dimension in which the diffusion occurs.

- that the water vapour in the fuel cell body is assumed to be saturated. In this way a direct relation between cell temperature and partial pressure of water vapour can be posed, Eq.(5):

$$p = f(T) \tag{5}$$

[Figure 2 about here.]

[Table 1 about here.]

2.3. Model Variables

Each molar flow shown on the figure 2 is determined by 8 variables (See Table 2). Next to the molar flows five other variables are shown on Fig.2 and described in table 2, the three heat fluxes and the electric power output, determined by voltage and current. The goal of the model is to predict the output flows (B, H and N), the generated electric power and the heat loss to the environment based upon the input flows (A, G and M). The other variables are intermediate stages which provide more understanding of the physical behaviour of the fuel cell. Based upon Fig. 2 all variables within the model are defined. The model exists out of 14 mass flows and 4 energy flows. Each mass flow exists out of 8 variables which describe the state of the flow (See Table 2). The energy flows are heat or electricity. The electric power is characterised by current and voltage.

[Table 2 about here.]

2.4. Model equations

For each control volume a mass and energy balance is used. The energy balances are closed by heat fluxes between neighbouring control volumes or between a control volume and the environment. This heat flux is modelled as a convective heat flux. Next to heat and mass transfer between control volumes, also electric energy, generated in the fuel cell body is transferred to the environment. An electrochemical model is used to describe the electric behaviour of the fuel cell. Finally the gas diffusion equations are used to relate the gas flows to the partial pressure of water vapour, which is assumed to be saturated in the fuel cell body.

2.4.1. Variables reduction

Since the intermediate flows are defined as component specific flows and based upon the nature of the inlet flows a number of molar fractions can be predefined, which will reduce the number of equations in the following model description.

2.4.2. Anode gas chamber

As shown in Fig.2, the fuel (A), a mixture of hydrogen and water vapour, enters the gas chamber, where the hydrogen diffuses into the gas diffusion layer (B). A part of the water, formed during the reaction in the fuel cell body, diffuses as water vapour back into the hydrogen gas chamber (C). A mixture of unused fuel and water vapour leaves the gas chamber to a next stage (D). Translating this to the molar flow and fractions within the anode gas chamber the following equations can be posed.

Molar balance:

$$F_A + F_D = F_B + F_C$$
$$F_A \cdot y_{H_2,A} = F_B \cdot y_{H_2,B} + F_C \quad (6)$$
$$F_A \cdot y_{w,A} + F_D = F_B \cdot y_{w,B}$$

As boundary condition in the simulation the fuel entering the (first) gas chamber is pure hydrogen and there is no hydrogen leaving the (last) gas chamber as unused fuel, because it is an end-of-pipe system.

Within the energy balance a heat transfer is defined from the fuel cell body to the gas chamber, since the gas flow and electrolyte flow through the channels are not insulated from each other. The heat transfer coefficient is modeled to be a function of the gas velocity in the gas chamber [11].

Energy balance:

$$F_A \cdot h_A + F_D \cdot h_D + Q_{anode} = F_B \cdot h_B + F_C \cdot h_C$$
$$Q_{anode} = hA_{FCB,an} * (T_{FCB} - T_{AGC}) \quad (7)$$
$$hA_{FCB,an} = c_5 \cdot v_{gasstream}^{c_6}$$

The calculation of the temperatures will be determined by the energy balance, since the calculation of the enthalpies is based upon temperature, molar fraction and pressure. See section 3.4.8 for more details on enthalpy calculation in Matlab. Next to these equations the assumptions offer extra relations, regarding pressure and temperature, which can be translated in the following equations

for the anode gas chamber.

Temperatures and pressures:

$$T_{anode} = T_B = T_C$$

$$p_A = p_B$$

$$p_C = \frac{p_A \cdot (F_A \cdot y_{H_2,A}) + p_B \cdot (F_B \cdot y_{H_2,B})}{F_A + F_B}$$

$$p_D = \frac{p_A \cdot (F_A \cdot y_{w,A}) + p_B \cdot (F_B \cdot y_{w,B})}{F_A + F_B}$$

(8)

2.4.3. Cathode gas chamber

The entering air contains oxygen, nitrogen and water vapour. There is a large excess of air because air is used to remove water vapour from the cathode. While oxygen diffuses to the fuel cell body, water vapour diffuses into the gas stream. The same remarks regarding heat transfer in the energy balance which were made for the anode are valid for the cathode.

Molar balance:

$$F_L + F_M = F_K + F_N$$

$$F_M \cdot y_{O_2,M} = F_K + F_N \cdot y_{O_2,N}$$

$$F_L + F_M \cdot y_{w,M} = F_N \cdot y_{w,N}$$

$$F_M \cdot y_{N_2,M} = F_N \cdot y_{N_2,N}$$

(9)

Energy balance:

$$F_L \cdot h_L + F_M \cdot h_M + Q_{cathode} = F_K \cdot h_K + F_N \cdot h_N$$

$$Q_{cathode} = hA_{FCB,cat} \cdot (T_{FCB} - T_{CGC})$$

$$hA_{FCB,cat} = c_5 \cdot v_{gasstream}^{c_6}$$

(10)

Temperatures and pressures:

$$T_{cathode} = T_K$$

$$T_{cathode} = T_N$$

$$p_M = p_N$$

$$p_K = \frac{p_M \cdot (F_M \cdot y_{O_2,M}) + p_N \cdot (F_N \cdot y_{O_2,N})}{F_M + F_N}$$

$$p_L = \frac{p_M \cdot (F_M \cdot y_{w,M}) + p_N \cdot (F_N \cdot y_{w,N})}{F_M + F_N}$$

(11)

The cathode outlet temperature is one of the main parameters on which the model is validated.

2.4.4. Anode gas diffusion layer

Between gas chamber and active surface a layer can be defined in which the diffusion or migration of the gases towards the reaction zone takes place. Since molar fractions are fixed the molar balance is very simple. The energy balance is built in the same way as the gas chambers. Temperatures are calculated similar to the gas chambers.

Molar balance:

$$F_C = F_E$$

$$F_D = F_F$$

(12)

Energy balance:

$$F_C \cdot h_C + F_F \cdot h_F = F_D \cdot h_D + F_E \cdot h_E$$

(13)

Temperature :

$$T_D = T_E$$

(14)

Diffusion equations and pressures:

In absence of a global pressure drop between the gas chamber and fuel cell

body, the driving force behind this migration is the concentration difference of the gases between the gas chamber and the boundary of the fuel cell body. This concentration difference is captured in the partial pressure difference between fuel cell body and gas chamber. The pressure of the intermediate flows in the model are in fact partial pressures. E.g. p_C is the partial pressure of hydrogen in the anode gas chamber and p_E will be the partial pressure of hydrogen at the boundary with the fuel cell body. The total pressure at each boundary is the sum of the pressure of the flows passing this boundary, since only water vapour and hydrogen are present at the anode side.

$$p_C + p_D = p_E + p_F \tag{15}$$

$$y_w + y_{H_2} = 1 \tag{16}$$

Taking this into account the Stefan-Maxwell equation (4) results in one independent differential equation, describing the diffusion and the lack of global pressure drop between the two boundaries (one of the assumptions, mentioned above).

$$\frac{dy_{H_2}}{dz} = \frac{RT}{P} \cdot \frac{y_{H_2} \cdot N_w - y_w \cdot N_{H_2}}{D_{Hw}}$$

with:

$$N_w = -a_1 \cdot F_D$$

$$N_{H_2} = a_1 \cdot F_C$$

$$a_1 = \frac{1}{n_{stack} \cdot n_{parallel} \cdot A_{cell}}$$

$$\tag{17}$$

The resulting differential equation is a first order (18)

$$\frac{dy_{H_2}}{dz} = \frac{RT}{P} \cdot \frac{y_{H_2} \cdot (N_w + N_{H_2}) - N_{H_2}}{D_{Hw}} \tag{18}$$

13

Since the diffusion occurs between the two boundaries, each boundary can be represented by a z-coordinate. As boundary condition the molar fraction in the gas chamber is set equal to a weighted mean of input and output flow, which was also the case for the (partial) pressure. Therefore at the anode side the following conditions have to be fulfilled.

$$y_{H_2} \cdot p_{tot} = p_C$$
$$y_w \cdot p_{tot} = p_D \tag{19}$$
$$z = 0$$

Since these partial pressures are a function of the molar flow, within the diffusion equations, an extra boundary condition is needed. This boundary condition is found at the side of the fuel cell body, which can be defined by the thickness of the diffusion layer, L_{GDF}. At this side, it is assumed that the partial pressure of the water vapour is equal to the saturation pressure in the fuel cell body, as a result of the earlier mentioned model assumptions. This results in the following equations:

$$y_{H_2} \cdot p_{tot} = p_E$$
$$y_w \cdot p_{tot} = p_F \tag{20}$$
$$p_F = p_{saturation,FCB}$$
$$z = L_{GDF}$$

2.4.5. Cathode gas diffusion layer

Similar to the anode gas chamber, at the cathode side a gas diffusion layer can be defined. Instead of diffusion of hydrogen and water vapour, at the cathode side there is a net diffusion of oxygen and water vapour.

Molar balance:

$$F_I = F_K \tag{21}$$
$$F_J = F_L$$

Energy balance:

$$F_K \cdot h_K + F_J \cdot h_J = F_I \cdot h_I + F_L \cdot h_L \tag{22}$$

Temperature :

$$T_I = T_L \tag{23}$$

Diffusion equations and pressures

Next to oxygen and water vapour also nitrogen exists in the cathode gas diffusion layer. Since nitrogen does not react in the fuel cell body there is no net nitrogen consumption of the fuel cell body and therefore no net transport of nitrogen over the diffusion layer. However the presence of nitrogen has an impact on the complexity of the formulation of the diffusion. The Stefan-Maxwell equation is used to formulate the diffusion equations.

$$\frac{dy_i}{dz} = \frac{RT}{P} \cdot \Sigma_j \frac{y_i \cdot N_j - y_j \cdot N_i}{D_{ij}} \tag{24}$$

which results in the following equations for oxygen, nitrogen and water vapour

$$\frac{dy_O}{dz} = \frac{RT}{P} \cdot \frac{y_O \cdot N_N - y_N \cdot N_O}{D_{ON}} + \frac{RT}{P} \cdot \frac{y_O \cdot N_w - y_w \cdot N_O}{D_{Ow}} \tag{25}$$

$$\frac{dy_w}{dz} = \frac{RT}{P} \cdot \frac{y_w \cdot N_N - y_N \cdot N_w}{D_{wN}} - \frac{RT}{P} \cdot \frac{y_O \cdot N_w - y_w \cdot N_O}{D_{Ow}} \tag{26}$$

$$\frac{dy_N}{dz} = -\frac{RT}{P} \cdot \frac{y_O \cdot N_N - y_N \cdot N_O}{D_{ON}} - \frac{RT}{P} \cdot \frac{y_w \cdot N_N - y_N \cdot N_w}{D_{wN}} \tag{27}$$

with

$$N_{O_2} = -a_1 \cdot F_K = -a_1 \cdot F_I \tag{28}$$

$$N_w = a_1 \cdot F_L = a_1 \cdot F_J$$

Since no net nitrogen flow is assumed in the model, N_N can be set to zero. Next to that the sum of the molar fractions is always one.

$$N_N = 0 \tag{29}$$

$$y_N = 1 - y_O - y_w \tag{30}$$

$$\frac{dy_N}{dz} = -\frac{dy_O}{dz} - \frac{dy_w}{dz} \tag{31}$$

Combining and deriving these equations results in a differential equation of the second degree for y_O. This results in the following differential equation which can be solved using similar boundary conditions as formulated for the anode diffusion.

At the side of the fuel cell body:

$$z = 0 \tag{32}$$

$$y_{w,FCB} = \frac{p_J}{p_{tot}} \tag{33}$$

$$p_J = p_{saturation,FCB} \tag{34}$$

At the side of the gas chamber:

$$z = L_{GDF} \tag{35}$$

$$y_{w,CGC} = \frac{p_L}{p_{tot}} \tag{36}$$

$$y_{O_2,CGC} = \frac{p_K}{p_{tot}} \tag{37}$$

2.4.6. Fuel cell body

Within the fuel cell body, the driving electrochemical reaction takes place. The mass and molar balance relates the hydrogen and oxygen consumption to the generation of water and electric current. The current is linked to the molar flows by Faraday's law.

Molar Balance:

$$\begin{aligned} F_G + \frac{I_{ref} \cdot n_{series}}{2Far} &= F_H + F_F + F_J \\ F_E &= \frac{I_{ref} \cdot n_{series}}{2Far} \\ F_I &= \frac{I_{ref} \cdot n_{series}}{4Far} \end{aligned} \tag{38}$$

Energy balance:

Within the fuel cell body the catalytic and separator layer are enclosed [13, 14, 15]. Although different layers exist in the fuel cell, in this paper the properties of the electrolyte/separator are taken to define the thermodynamic behaviour

16

of the fuel cell body. The mass flows between fuel cell body and gas chamber however will only consist of gas in accordance to the boundary conditions of the gas diffusion layers. This will affect the enthalpy of these streams and will limit the mass or molar flow, because the partial pressure cannot exceed the saturation pressure.

$$F_G \cdot h_G + F_E \cdot h_E + F_I \cdot h_I =$$
$$F_H \cdot h_H + F_F \cdot h_F + F_J \cdot h_J + Q_{FCB} + P_e$$
$$Q_{FCB} = Q_{FCB,sur} + Q_{FCB,cat} + Q_{FCB,an} \tag{39}$$
$$Q_{FCB,surr} = hA_{FCB,surr}.(T_{FCB} - T_{surr})$$
$$h_F = h_J$$

The energy balance of the fuel cell body consists not only of incoming and outgoing mass streams and heat flows, but also of an electric power output. This output is more detailed in the electrochemical model.

2.4.7. Electrochemical model

The electrochemical model, presented in [11], is used. Since a few parameters were adapted within the model the used equations are summarized.

$$P_e = U \cdot I \tag{40}$$

$$U = E_{Nernst} - \eta_{act} - \eta_{res} - \eta_{diff} \tag{41}$$

$$E_{Nernst} = -\frac{\Delta G_0}{2Far} + \frac{RT_{cell}}{2Far}\left[ln\left(p_{H_2}\right) + \frac{1}{2}ln\left(p_{O_2}\right)\right] \tag{42}$$

$$\eta_{act} = \frac{R \cdot T}{\alpha \cdot n \cdot Far}ln\left(\frac{\frac{I_{cell}}{A}}{j_0}\right) \tag{43}$$

$$\eta_{res} = R_e \cdot I_{cell} \tag{44}$$

$$\eta_{diff} = \frac{R \cdot T}{\alpha \cdot n \cdot Far}ln\left(\frac{j_L}{j_L - \frac{I_{cell}}{A}}\right) \tag{45}$$

$$j_0 = c_1 \cdot exp\left(\frac{-c_2}{T_{cell}}\right) \tag{46}$$

$$R_e = c_3 - c_4 \cdot T_{cell} \tag{47}$$

2.4.8. Discussion on parameter estimation

[Table 3 about here.]

Table 3 contains all used semi-empiric parameters, which were used to tune the model. Since the new model is built upon the base of the model in [11], the same values were used in a first approach. Due to the extra layer at each side the parameters regarding the heat transfer coefficient towards anode and cathode will be different. This difference is found in c_5. Its value is reduced, since part of the heat transfer from the electrolyte into the gas stream is already included in the energy balance of the diffusion layer. Next to this difference a new parameter is introduced, namely L_{GDF}. To determine an acceptable range for L_{GDF} a comparison was made with Jo et al.[23]. In this paper values from 0.05 to 0.55mm were found to be representative for the thickness of the gas diffusion layer. These variations however had no significant influence on performance. Since the model, presented in this paper, has a gas diffusion layer, but no catalyst layer, the gas diffusion layer is chosen to be thicker to include the diffusion resistance of the catalyst layer. The catalyst layer is 2 to 5 times thinner than the diffusion layer and the diffusion coefficients are 10 to 100 times larger for gas diffusion compared to diffusion through liquid [14]. Therefore, in this model a value between 0.05 and 1cm is acceptable.

2.5. Implementation of the model in Matlab

For the implementation of the model, Matlab is chosen. Originally the model was built in Aspen Custom Modeler [11]. Aspen Custom Modeler however isn't built to deal with complex mathematical problems, which are sensitive to small distortions. The diffusion equations lead to an increased complexity and therefore Matlab is chosen, which is more apprioriate for the scope of our work. As a consequence the libraries of Aspen aren't available anymore to calculate all the necessary physical properties. As a solution, the different thermodynamic properties of Aspen Custom Modeller are translated into constants or linear

functions so they could be implemented in Matlab. For the gasses hydrogen, nitrogen and oxygen this is acceptable, since they are considered to be ideal. For the enthalpy and Gibbs free energy calculations of water (vapour) a published Matlab function by Magnus Holmgren [24] is used. Table 4 presents an overview of the used constants in the linear expression (48) to calculate enthalpy.

$$h_{gas} = c_{gas} \cdot T(°C) + b_{gas} \tag{48}$$

[Table 4 about here.]

Also the diffusion constants in the Stefan-Maxwell equations need to be imported. In a first approach they were imported as a constant from the libraries of Aspen Custom Modeller. However, because the diffusion is a function of temperature, already mentioned by Jo et all(2000) [23], this correlation is included into the model, Eq. (49).

$$D(T) = D_0 \cdot T^{2,334} \tag{49}$$

3. Model validation

The model is validated using experimental data which were generated with the AFC system described in detail in [11, 25]. Part of these experimental results were discussed in [11]. Further data analysis is performed to evaluate the new element in the model, i.e. the water management.

3.1. Experimental set-up

[Figure 3 about here.]

Figure 3 shows a schematic view of the experimental set-up. Table 5 gives a brief description of the main operating parameters, marked on Fig.3.

[Table 5 about here.]

For a detailed description of the parameters a to h in the experimental set-up we refer to earlier work, where the same experimental data were used to validate a previous model [11]. Next to the already discussed parameters the level of electrolyte is measured (point i). The measurement however is not that precise, because the water surface is not stable. This is caused by the KOH-pump which switches between working steps and by the output air flow which passes over the electrolyte tank. Only an evaluation of the water level - with consideration of changes in electrolyte flow (point e) - over a long period of time will indicate when there is a net evaporation of water (electrolyte) or when there is a net formation of liquid water during this period of time.

3.2. Model validation

Current - which is directly proportional to the input hydrogen flow - input air flow rate, input electrolyte flow rate and input electrolyte temperature are used as input parameters for model validation. The model is used to predict electrical performance, thermal behaviour and water management. The model will be validated on these three aspects, which can be characterized by voltage, output temperatures for both electrolyte and air and by output flow rate of the liquid electrolyte. The validation is performed in two stages.

- First the model is compared with the previous model [11] and validated regarding the prediction on voltage and thermal behaviour, using a selection of experimental data shown in Table 6. The selection of these working points is described in [11].

- Secondly the water management is validated by selecting a long period in which the fuel cell is relatively stable and the electrolyte level is monitored.

3.2.1. Validation with existing experimental data

[Table 6 about here.]

As described in ref. [11], all measured parameters are subject to uncertainties. Data analysis led to a data set of 50 working points. The measured parameters,

which are used as model input, are illustrated by a representative selection of data points. This selection, shown in Table 6, is based on current and electrolyte temperature, the two most determining input parameters. The first two working points are representative for the range in which the data were obtained: the first one represents the lower bound and the second one the upper bound for both current and electrolyte temperature. The next four data points are all measured at the same average current, over a wide range of electrolyte temperatures. The last four are all measured at about the same average electrolyte temperature over a wide range of currents. The measured and modeled output parameters of these ten data points are shown in figures 4, 5 and 6. A complete data set with all 50 measured and modelled data points will be held available by the authors. In each of these figures the experimental data are compared to the model also ref. [11] and to this new model, described in this paper.

- The experimental output is represented by dots with error bars, which represent the instability on the measurement, similar to the variation in the input value, shown in Table 6.

- The output of the model is represented by a floating bar. The line in the middle of this bar represents the modeled output of the mean input parameters listed in Table 6. To include the measurement error on the model input a set of model experiments were executed. In this set all possible combinations of extreme input values for each input parameter were used as input for the model, based upon the mean values and measurement errors, listed in Table 6. In the end, the maximum and minimum result were considered to be the upper and lower bound of the model output.

- The model in [11] is represented with a circle. For this model the measurement error on the input parameters was not taken into account.

Electrical performance, voltage:

[Figure 4 about here.]

In Figure 4 the prediction on electric performance is shown. The data is arranged by ascending current and electrolyte temperature, in case of similar currents (data points 7 to 10). The model shows a better performance on prediction of the voltage, compared to [11]. For two data points no overlap is found between the experimental and the modeled voltage. This is however acceptable because in the complete set of 50 data points these are indeed the only two points, where no overlap is found. In these points the new model has a smaller deviation than the previous model. Next to this, both for the experimental as for the modelled voltage, a similar influence of the current is shown in Fig.4. The same result is shown regarding the positive influence of the electrolyte temperature (data point: 7 to 10) on the electrical performance or total voltage. The model is therefore representative in predicting the voltage, including the effect of temperature and current on electrical performance.

Thermal behaviour, electrolyte temperature:

[Figure 5 about here.]

In Figures 5 and 6 the thermal behaviour is shown. Figure 5 shows the prediction of the output electrolyte temperature. The model has comparable results to [11], in predicting the electrolyte temperature. For two data points there is no overlap. In the complete data set three working points show no overlap. The deviation however is limited to a few degrees. The higher the electrolyte temperature, the higher the output electrolyte temperature. This is visible both in the experimental as in the modeled results. In the discussion on experimental results in [11] was already mentioned that the temperature rise in the electrolyte grows with higher current. This effect is visible in the modeled output, but is not very clear in the shown experimental results (data points 3 to 6).

Thermal behaviour, air temperature:

[Figure 6 about here.]

Figure 6 shows the prediction of the output air temperature. For all 50 working points there is an overlap. Next to that, the relation with the electrolyte temperature is noticeable, both in the measurements as in the model. Therefore,

the model is acceptable to predict thermal behaviour. Still the prediction of the air temperature is sensitive to the air flow, the parameter with the highest error range. As a result the modelled output shows a large difference between upper and lower boundary. The most remarkable result is the lower bound in working point 9. This represents an impossible situation, due to the high standard deviation in the measured air flow. The point however shows one of the limitations of the model, since it is assumed that the air flow is controlled to be at least sufficient to compensate the hydrogen input in Faraday's law. This assumption is not fulfilled in point 9, so the model cannot be used with those input conditions.

3.2.2. Validation on the water management

[Figure 7 about here.]

[Table 7 about here.]

To validate the model regarding the water management, the level of the electrolyte in the KOH-tank is monitored in time over the duration of the experiments (Fig.7). In this time period it was possible to determine 6 periods in which the electrolyte level shows a clear and steady change and in which the variation on the inlet conditions was relatively stable (Table 7). These conditions were used as input data for our model to predict the water production in the electrolyte flow, which will result in a rise (or reduction) of the electrolyte level in the KOH-tank. If the model is representative to reflect the measurements, the modeled water production is directly proportional to the speed at which the measured electrolyte level rises. In Figure 8 the model results for the formation of liquid water in the electrolyte flow (Y-axis) are set as a function of the measured rise per unit of time of the electrolyte level in the KOH-tank (X-axis). These data sets are represented by the triangles, which are expected to be in a straight line through the origin. However, when the electrolyte level drops (periods 2.5 and 6 in Table 7), the model overestimates the formation of liquid water in the electrolyte.

23

[Figure 8 about here.]

At high currents (periods 2 and 6 in Table 7) the model predicts a rise in electrolyte level due to the high water production. The measurements show however a drop in electrolyte level. Table 7 shows that the positive effect of the current on the water formation is almost neglectable compared to the negative effect of the air flow and electrolyte temperature. According to the measurements, air flow rate and temperature are the most determining parameters regarding rise or decrease of the electrolyte level. This could be due to the fact that the output air, which is not saturated, passes the tank. Assuming that this passage will result in an increased relative humidity ($RH\%$) of the output air, more water will be evaporated at higher air flow rate and higher temperature, resulting in a lower electrolyte level.

3.2.3. Model extension for electrolyte tank

To verify this the evaporation in the electrolyte tank is modelled as a function of the following parameters:

- electrolyte temperature

- electrolyte flow

- air flow

- air temperature

- relative humidity of air

- percentage of evaporation: 0 means no evaporation - 100 means that the air is completely saturated

Only this last parameter could be fitted to the results. Since it is reasonable that the KOH tank has an influence, but complete saturation will not be reached, the parameter will be higher than 0 and lower than 100. A best fit could be found at about 40%. Taking the error bars into account, the model already shows good results for an evaporation percentage of 30% to 65%. At lower percentages the

effect of the tank is too small. At higher evaporation percentages the model of the KOH-tank overcompensates the effect of the fuel cell on the water balance. With the evaporative effect of the KOH-tank added to the model validation it is shown that the model predictions on the production of liquid water are confirmed by the experimental results (See figure 8). These are presented by the dots, which are aligned including the origin. This means that the model extension is sufficient and important to understand the results of the experimental set-up.

4. Analysis of the water management

With the validated model a sensitivity analysis is performed to gain insight in the effect of every input parameter on the water management within the fuel cell. For the analysis the influence of seven parameters is examined by simulation (See Table 8). The cumulated influence of the first two parameters, current and electrolyte temperature with any other parameter is examined at every new condition, determined by the other five parameters. Table 8 presents an overview of the different inputs that are analysed below.

[Table 8 about here.]

4.1. Influence of the electrolyte

To evaluate the influence of the electrolyte, both electrolyte flow rate and electrolyte temperature at the input were set at different values. The electrolyte flow shows no significant influence on the water management. The electrolyte temperature however has a large impact on the water management.

[Figure 9 about here.]

In figure 9 is shown that at low electrolyte temperature almost no water vapour diffuses and that the formed liquid water is proportional to the current, which is directly linked to the generated water, Eq. (38) (See also figure 10). The impact of the electrolyte temperature on the evaporation is proportional to its

25

impact on the saturation pressure. At least a temperature of about 55°C has to be reached to avoid net rise of liquid water in the electrolyte flow. At lower temperatures the saturation pressure drops rapidly. Because of this the driving force for the water vapour diffusion is strongly reduced. As a result liquid water builds up due to the formation of water, which is not transported out of the fuel cell by diffusion. For the same reason, but now in the opposite direction, there is a net evaporation at temperatures higher than 75°C, at least for currents within nominal working range (20A to 80A). To avoid dry out of the fuel cell, 75°C is to be set as a maximum temperature when working with dry or cold air. This will limit the electric efficiency since this is higher at higher temperature [11].

4.2. Influence of current

[Figure 10 about here.]

At low temperature current has no significant influence and all formed water will end up in the electrolyte flow. Figure 10 shows that for every input electrolyte temperature higher than the minimum value (about 55°C, See Section 4.1) a current can be found at which all formed water is evaporated and diffuses into the gas streams. This is interesting regarding steady state working points.

4.3. Influence of the input air

To understand the influence of the air stream, three parameters were evaluated:

- the air ratio or the actual air flow in relation to the necessary air flow

- the relative humidity

- the air temperature

[Figure 11 about here.]

[Figure 12 about here.]

26

Figure 11 shows that a higher air ratio has a negative effect on the net formation of liquid water. The relative impact of an increased air ratio reduces after a ratio of 2,5 to 4 (See Fig. 11). Naturally, the impact of the air ratio on the evaporation of the electrolyte tank is directly related, as shown in the model extension for the electrolyte tank (See Section 3.2.2). The air ratio can be used as a control parameter for the water management within a small range within the stack itself (1 - 2,5). If the output air passes over the electrolyte tank, as in the used experimental set-up of the AFC-system, the air ratio can be a useful control paramater in a much wider range.

Next to the air ratio, the temperature and relative humidity will be of importance. Their effect however, is relatively low. If the input air is dry, the air temperature has only a very small positive effect on the diffusion, which results in a lower net liquid water formation. The relative humidity only has a large impact at high input air temperature (See Fig. 12). At lower temperature the water vapour content of saturated air is a lot lower and will have no significant influence on the water vapour content of the heated output air stream. As discussed earlier(See Section 4.1), to avoid dry out of the fuel cell a maximum temperature of the electrolyte has to be respected. However, this statement was posed using dry and cold air as inlet for the cathode. In Fig. 12 is shown that at higher electrolyte temperature it is still possible to maintain water content of the electrolyte flow, if hot humidified air is used as input for the fuel cell. Because electrolyte temperature has a positive effect on the fuel cell performance [11], this could increase the efficiency of the fuel cell.

5. Conclusion

A model of an alkaline fuel cell is created in Matlab. The model predicts the thermodynamic behaviour and water management of the fuel cell and is validated with experimental data from a system designed for CHP-applications. The influence of the input parameters on the water management is investigated.

- To maintain the concentrations within the electrolyte, a minimum electrolyte temperature has to be reached (about 55°C) to operate at low current.

- Higher currents will require higher input temperatures of the electrolyte to maintain the electrolyte concentration.

- The electrolyte temperature at a given current can be increased without dry out using hot humidified air.

- An air ratio higher than 2.5 is no more effective as a control paramater to maintain electrolyte concentration within the fuel cell.

Acknowledgements

References

[1] M. Pehnt, *Environmental impacts of distributed energy systems-The case of micro cogeneration*, Environmental science and policy II (2008),25-37.

[2] M. De Paepe, P. D'Herdt, D. Mertens, *Micro-CHP systems for residential applications*, Energy Conversion and Management, Volume 47, Issues 18-19, November 2006, Pages 3435-3446.

[3] K. Alanne, A. Saari, *Sustainable small-scale CHP technologies for buildings: the basis for multi-perspective decision-making*, Renewable and Sustainable Energy Reviews,Volume 8, Issue 5 (October 2004) Pages 401-431

[4] A.D. Hawkes, D.J.L. Brett, N.P. Brandon, *Fuel cell micro-CHP techno-economics*, International Journal of Hydrogen Energy 34(2009)9545-9557.

[5] I. Staffell, A. Ingram, *Life cycle assessment of an alkaline fuel cell CHP system*, International Journal of Hydrogen 35(2010) 2491-2505.

[6] H.I. Onovwiona, V.I. Ugursal, *Residential cogeneration systems: review of the current technology*, Renewable and Sustainable Energy reviews 10 (2006) 389-431.

[7] I. Staffell, *A review of small stationary fuel cell performance* , $http : //wogone.com/iq/review_off uel_cell_p erformance.pdf$ (2009) [cited December 2010].

[8] G.F. Mclean,T. Niet,S. Prince-Richard,N. Djilali, *An assessment of alkaline fuel cell technology*, International Journal of Hydrogen Energy 275(2002)507-526.

[9] E. Gulzow, J.K. Nor, P.K. Nor and M. Schulze, *A renaissance for alkaline fuel cells* The fuel cell review, Volume 3 Issue 1 (2006).

[10] E. Gulzow,M. Schulze, U. Gerke, *Bipolar concept for alkaline fuel cells* International Journal of Power Sources 156(2006)1-7.

[11] I. Verhaert, M. De Paepe, G. Mulder, *Thermodynamic Model for an Alkaline Fuel Cell*, Journal of Power Sources 193(1) (2009); 193(1) 233-240.

[12] G. Mulder, *Alkaline Fuel Cells - Overview*, Encyclopedia of Electrochemical Power Sources (2009), Pages 321-328.

[13] M.C. Kimble and R.E. White, *A Mathematical Model of a Hydrogen/Oygen Alkaline Fuel Cell*, J. Electrochem. Soc., Vol. 138, No. 11, (November 1991)3370-3382.

[14] J.-H. Jo, S.-C. Yi, *A computational simulation of an alkaline fuel cell*, Journal of Power Sources 84 (1999) 87-106.

[15] M. Duerr, S. Gair, A. Cruden, J. McDonald, *Dynamic electrochemical model of an alkaline fuel cell stack*, Journal of Power Sources, Volume 171, Issue 2, (27 September 2007) 1023-1032.

[16] S. Rowshanzamir, M. Kazemeini and M.K. Isfahani. *Mass balance and water management for hydrogen-air fuel cells*, Journal of Hydrogen Energy, Volume 23, Issue 6 (June 1998) 499-506.

[17] H.Huisseune, A. Willockx, M. De Paepe, *Semi-empirical along-the-channel model for a proton exchange membrane fuel cell* International Journal of Hydrogen Energy, Volume 33, Issue 21 (November 2008)6270-6280.

[18] J.Wu, X.Z. Yuan, H. Wang, M. Blanco, J.J. Martin, J. Zhang, *Diagnostic tools in PEM fuel cell research: Part I Electrochemical techniques*, International Journal of Hydrogen Energy 33 (2008)1735-1746.

[19] B.Y.S. Lin, D.W. Kirk, S.J. Thorpe, *Performance of alkaline fuel cells: A possible future energy system?*, Journal of Power Sources 161 (2006). 474-483.

[20] R. O'Hayre, S.-W. Cha, W. Colella and F.B. Prinz, Fuel Cell Fundamentals, Chapter 6: Fuel Cell Modelling, (2006) pp 169-192.

[21] J.C. Amphlett, R.F. Mann, B.A. Peppley, P.R. Robergy, A. Rodrigues, *A model predicting transient responses of proton exchange membrane fuel cell*, Journal of Power Sources 1996; 61(1-2) 183-188.

[22] C. Depcik, D. Assanis *A universal heat transfer correlation for intake and exhaust flows in an spark-ignition internal combustion engine*, SAE Paper 2002-01-0372.

[23] J.H. Jo, S.-K. Moon and S.-C. Yi, *Simulation of influences of layer thickness in an alkaline fuel cell*, Journal of Applied Electrochemistry 30 (2000),1023-1031.

[24] M. Holmgren, *Matlab function: X STEAM*, www.x-eng.com (2006-01-20).

[25] G. Mulder, P. Coenen, A. Martens, J. Spaepen, *The development of a 6 kW fuel cell generator based on alkaline fuel cell technology*, International Journal of Hydrogen Energy, Volume 33, Issue 12 (June 2008) 3220-3382.
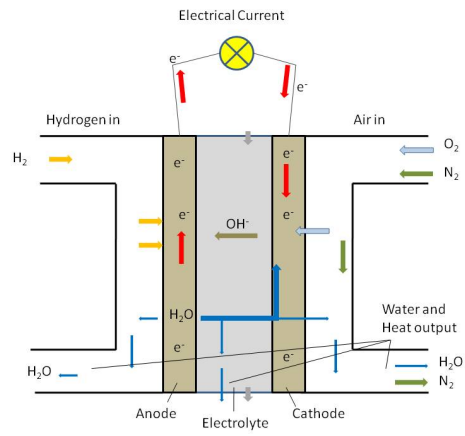
List of Figures
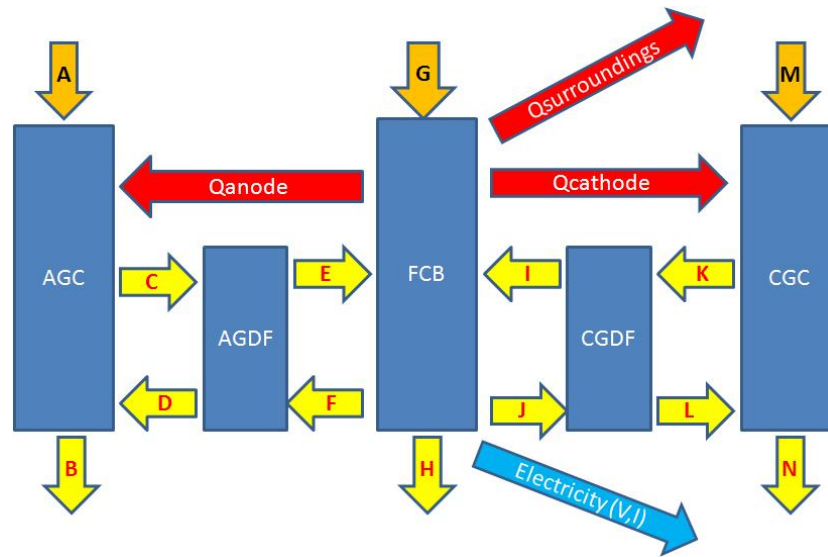
Figure 1: Working Principle of an Alkaline Fuel Cell

Figure 2: Lay-out of the alkaline fuel cell model (See Table 1 for a detailed description).
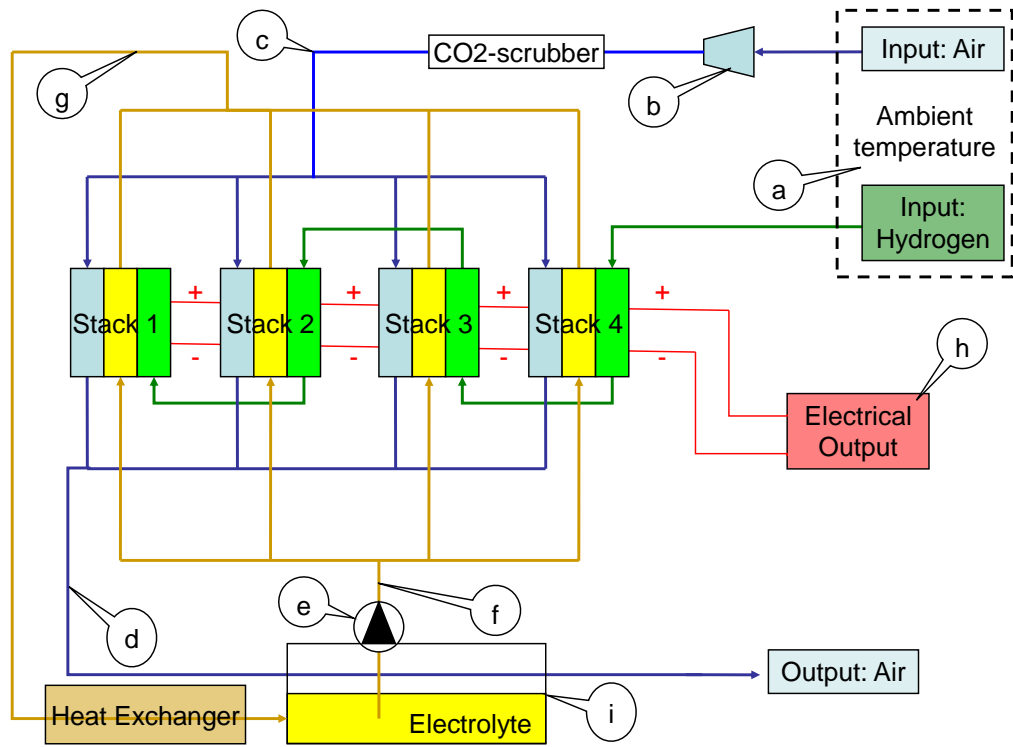
Figure 3: Experimental set-up of the AFC-system, in which the main operating parameters are marked and described in Table 5.
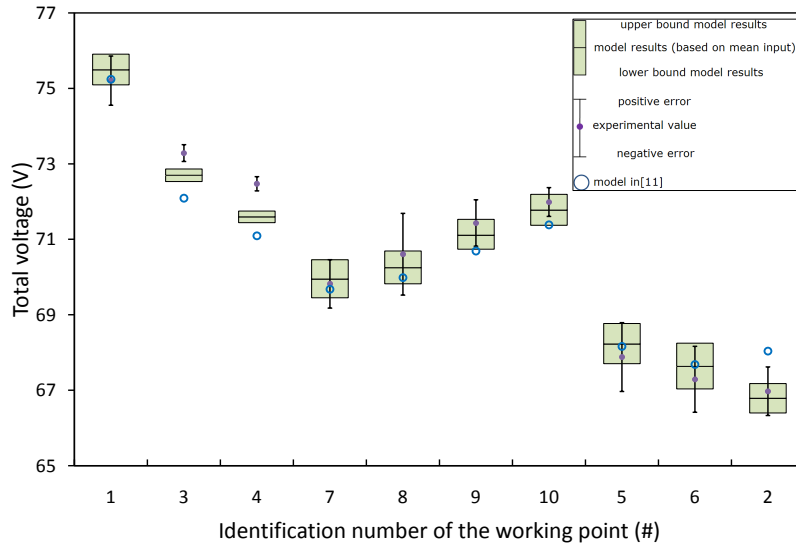
Figure 4: Model verification on electric performance (voltage) with the working points (See Table 6) arranged by ascending current and temperature in case of equal current (points 7 to 10). For every point the model prediction (floating bars) is compared to the experiments (dots) and the model in [11](circles).
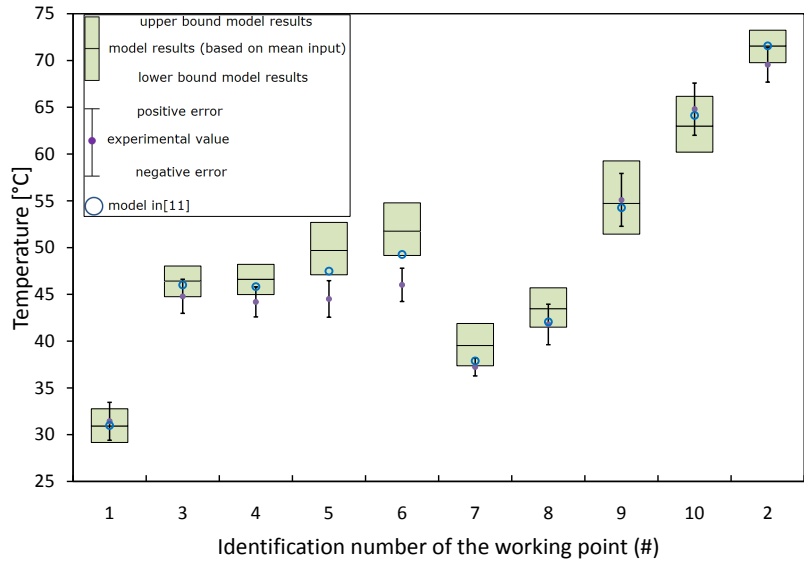
Figure 5: Model verification, output electrolyte temperature. Data points 3 to 6 have all the same input electrolyte temperature and are arranged by ascending current. Data points 7 to 10 have all the same current and are arranged by ascending input electrolyte temperature. Data points 1 and 2 are the two most extreme values, considering current and input electrolyte temperature. For every point the model prediction (floating bars) is compared to the experiments (dots) and the model in [11](circles).
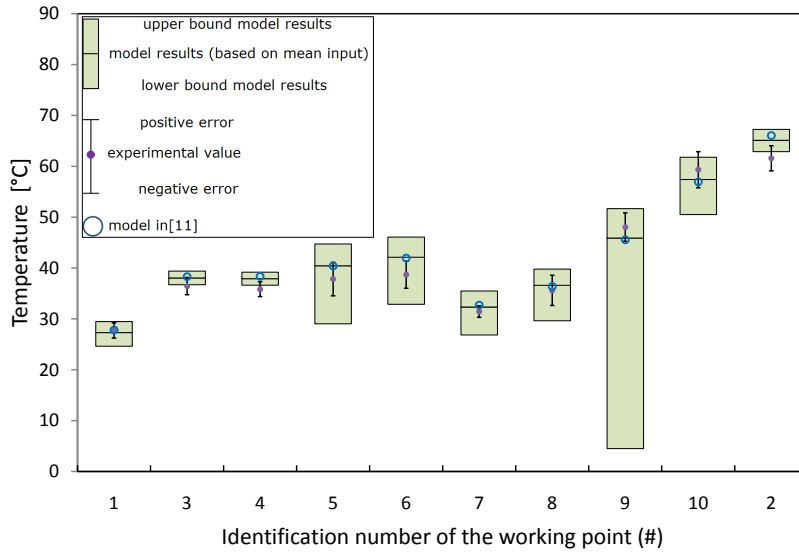
Figure 6: Model verification, output air temperature. Data points 3 to 6 have all the same input electrolyte temperature and are arranged by ascending current. Data points 7 to 10 have all the same current and are arranged by ascending input electrolyte temperature. Data points 1 and 2 are the two most extreme values, considering current and input electrolyte temperature. For every point the model prediction (floating bars) is compared to the experiments (dots) and the model in [11](circles).
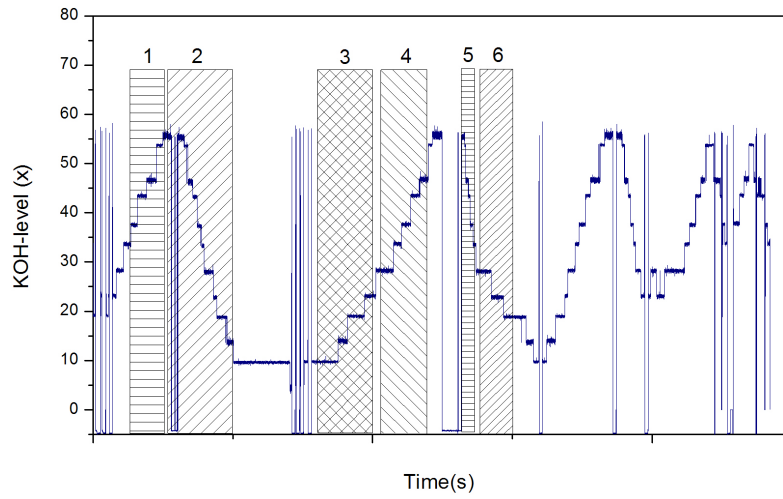
Figure 7: Measured fluctuation of the electrolyte level in the KOH-tank during time of the experiments. Six periods are selected in which the input parameters are relatively stable and marked on the figure. These 6 periods are described in Table 5
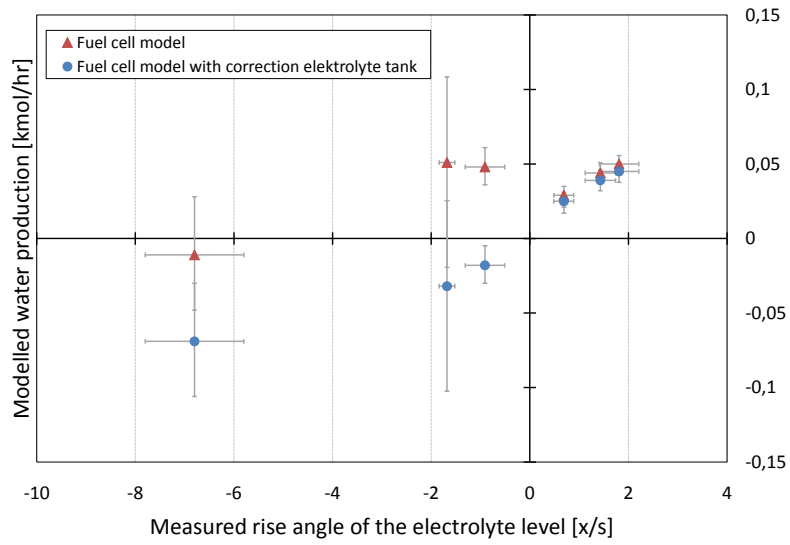
Figure 8: Prediction of liquid water production vs measured rise of electrolyte level. Both for the fuel cell model (triangle) as for the extended model with the electrolyte tank (dots) the model results are set as a function of the measurements.
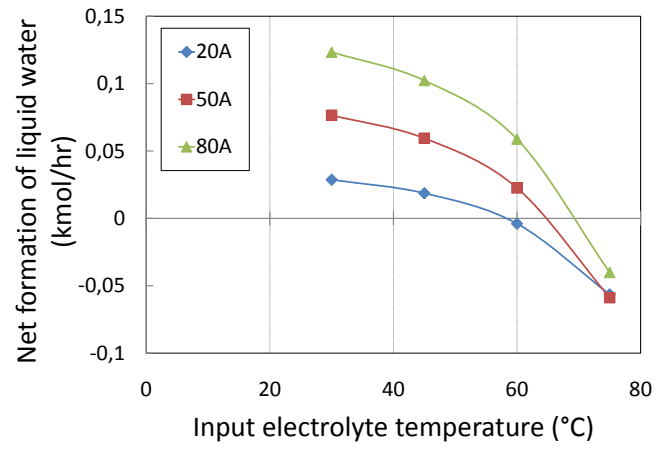
Figure 9: Sensitivity of liquid water production to electrolyte temperature at three different currents.
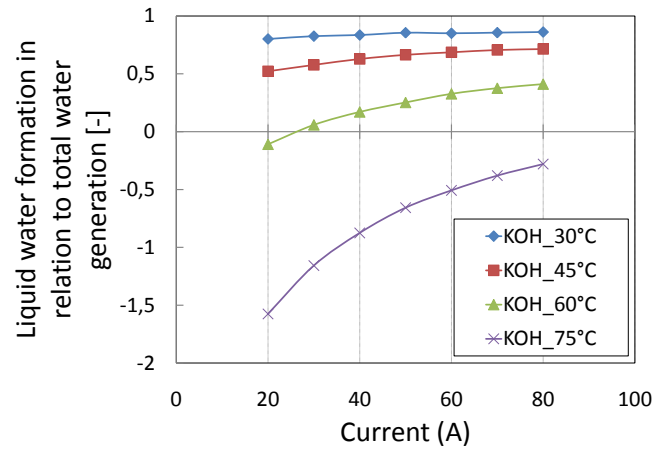
Figure 10: Sensitivity of liquid water production to total current at four different electrolyte temperatures.

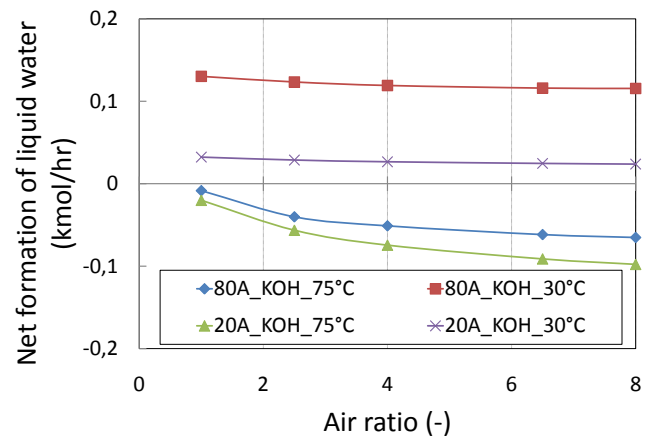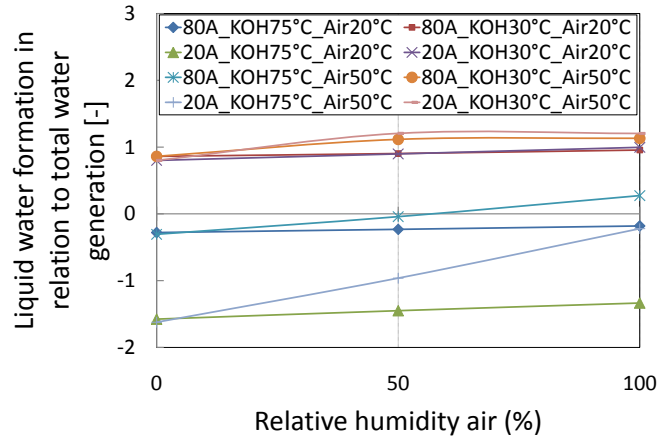Figure 11: Sensitivity of liquid water production to air ratio.

Figure 12: Sensitivity of liquid water production to relative humidity and air temperature. For 8 different combinations of currents (20A or 80A), electrolyte temperature (30°C or 75°C) and air temperature (20°C or 50°C) the net formation of liquid water is set as a function of the relative humidity of the input air.

List of Tables

Name	Description
AGC	Anode gas chamber, part of the hydrogen flow channel in contact with the fuel cell.
AGDF	Anode gas diffusion layer, boundary layer where gasses (hydrogen and water vapour) diffuse into and out of the fuel cell.
FCB	Fuel cell body, existing out of both catalytic layers (with the electrodes) and out of the separator layer (the electrolyte, in which the ion transport takes place.)
CGDF	Cathode gas diffusion layer, boundary layer where gasses (oxygen and water vapour) diffuse into and out of the fuel cell.
CGC	Cathode gas chamber, part of the air flow channel in contact with the fuel cell.
A	Input molar flow at the anode, containing hydrogen (and water vapour).
B	Output molar flow at the anode, containing water vapour (and hydrogen).
C	Molar flow of hydrogen, diffusing from AGC into FCB, at the boundary with AGC.
D	Molar flow of water vapour, diffusing from FCB into AGC, at the boundary with AGC.
E	Molar flow of hydrogen, diffusing from AGC into FCB, at the boundary with FCB.
F	Molar flow of water vapour, diffusing from FCB into AGC, at the boundary with FCB.
G	Input molar flow for FCB, containing electrolyte (water).
H	Output molar flow from FCB, containing electrolyte (water).
I	Molar flow of oxygen, diffusing from CGC into FCB, at the boundary with FCB.
J	Molar flow of water vapour, diffusing from FCB into CGC, at the boundary with FCB.
K	Molar flow of oxygen, diffusing from CGC into FCB, at the boundary with CGC.
L	Molar flow of water vapour, diffusing from FCB into CGC, at the boundary with CGC.
M	Input molar flow for CGC, containing (wet)air
N	Output molar flow from CGC, containing wet air
Q_{anode}	Energy flow: (convective) heat transfer from FCB to AGC.
$Q_{cathode}$	Energy flow: (convective) heat transfer from FCB to CGC.
$Q_{surroundings}$	Energy flow: heat losses to the environment.
Electricity	Energy flow: generated electricity.

Table 1: Description of the control volumes and the molar and energy flows in Fig.2

Variables	Symbol	Unit
Molar Flow	F	$kmol/hr$
Temperature	T	$°C$
Pressure	p	bar
Enthalpy	h	$GJ/kmol$
Molar Fraction Hydrogen	y_{H_2}	
Molar Fraction Oxygen	y_{O_2}	
Molar Fraction Water(Vapour)	y_w	
Molar Fraction Nitrogen	y_{N_2}	

Table 2: List of variables in each mass (molar) stream

Parameter	Value [11]	New Model
j_L	$2000A/m^2$	$2000A/m^2$
α	0.1668	0.1668
c_1	$174512A/m^2$	$174512A/m^)$
c_2	$5485K$	$5485K$
c_3	0.0045Ω	0.0045Ω
c_4	$5.9e - 5\Omega/K$	$5.9e - 6\Omega/K$
c_5	$3.375e - 3$	$1.5e - 3$
c_6	1.5	1.5
hA_{sur}	$51.2W/K$	$51.2W/K$
L_{GDF}		$0.2cm$

Table 3: List of the used semi-empiric parameters

Gas	b $[GJ/kmol]$	c $[GJ/(kmol \cdot^\circ C)]$
Hydrogen	$-7.22573286 \cdot 10^{-4}$	$2.89388143 \cdot 10^{-5}$
Nitrogen	$-7.28014 \cdot 10^{-4}$	$2.91195 \cdot 10^{-5}$
Oxygen	$-7.32343 \cdot 10^{-4}$	$2.92833 \cdot 10^{-5}$

Table 4: Constants for enthalpy calculation

Parameter	Description	Measuring method
a	Ambient temperature (input temperature for air and hydrogen supply)	Direct
b	Air flow	Indirect
c	Air temperature	Estimated
d	Output air temperature	Direct
e	Electrolyte flow	Indirect
f	Input electrolyte temperature	Direct
g	Output electrolyte temperature	Direct
h	Total voltage, Current, cell voltages	Direct
i	Level of the electrolyte in the tank	Direct

Table 5: List of operating parameters of the AFC-system, marked on Fig.3

Identification number of working point	Current A	Electrolyte input flow kmol/hr	Electrolyte input temperature °C	Air input flow kmol/hr
1	18.5 ± 0.9	22.1 ± 0.0	29.4 ± 1.8	0.3 ± 0.2
2	73.3 ± 1.8	19.8 ± 0.0	68.3 ± 1.9	0.9 ± 0.1
3	33.3 ± 0.2	21.8 ± 0.0	44.4 ± 1.9	0.3 ± 0.0
4	38.2 ± 0.2	22.2 ± 0.6	43.7 ± 1.8	0.3 ± 0.0
5	55.9 ± 2.2	20.0 ± 0.0	42.9 ± 2.2	0.4 ± 0.4
6	59.9 ± 2.8	19.5 ± 0.9	44.3 ± 1.6	0.5 ± 0.3
7	43.4 ± 1.9	21.3 ± 0.0	34.0 ± 1.9	0.4 ± 0.3
8	43.4 ± 1.6	20.4 ± 0.0	38.6 ± 1.7	0.5 ± 0.4
9	43.4 ± 0.8	21.8 ± 0.0	52.5 ± 3.4	0.4 ± 0.3
10	43.4 ± 1.1	21.5 ± 0.0	63.7 ± 2.9	0.6 ± 0.3

Table 6: Selection of measured data point for model input

| Period | Duration | Input conditions (mean +- standard deviation) | | | | Evolution of KOH Level |
		Current (A)	KOH flow (kmol/hr)	KOH temp. (°C)	Air Flow (kmol/hr)	
1	$5000s$	36.9 ± 2.8	21.5 ± 0.5	38.4 ± 0.3	0.31 ± 0.05	↗
2	$12500s$	82.2 ± 13.5	20.5 ± 1.5	63.5 ± 8.1	0.74 ± 0.23	↘↘
3	$10000s$	21.8 ± 2.4	24.2 ± 5.4	32.8 ± 3.4	0.32 ± 0.05	↗↗
4	$6500s$	31.5 ± 2.4	$21,4 \pm 0.7$	35.6 ± 2.6	0.29 ± 0.04	↗↗
5	$2000s$	45.9 ± 17.3	19.8 ± 1.0	65.3 ± 2.6	0.78 ± 0.15	↘↘↘
6	$5000s$	79.9 ± 2.2	21.3 ± 0.9	64.0 ± 0.7	0.6 ± 0.19	↘

Table 7: Experimental data for validation of water management

Parameter	average	minimum	maximum	step size
Current	20A-80A	20A	80A	10A
Input electrolyte temperature	30°C-75°C	30°C	75°C	15°C
Input air temp	20°C	5°C	65°C	15°C
Input air RV%	0	0%	100%	50%
Input air flow (air ratio)	2.5	1	8	1.5
Input electrolyte flow	20.5 kmol/hr	19	22	1.5 kmol/hr
Temperature surroundings	20	-10°C	50°C	15°C

Table 8: Description of the sensitivity analysis